Heliyon 6 (2020) e03902

Contents lists available at ScienceDirect

Heliyon

journal homepage: www.cell.com/heliyon

Research article

Numerical and experimental study on wind environment at near tower region of a bridge deck

Q. Zhou [a,*], L.D. Zhu [b]

[a] Guangdong Engineering Center for Structure Safety and Health Monitoring, Shantou University, No. 243 Daxue Road, Shantou, Guangdong Province, China
[b] State Key Laboratory for Disaster Reduction in Civil Engineering, Tongji University, No. 1239 Siping Road, Shanghai, China

ARTICLE INFO

Keywords:
Civil engineering
Construction engineering
Coastal engineering
Heat transfer
Computational mechanics
Mechanical systems
Wind environment
LES
Wind tunnel test
Windshield barrier
Equivalent wind speed

ABSTRACT

The Large Eddy Simulation (LES) turbulence model was used to investigate the wind environment over the deck near bridge tower and was verified using the wind tunnel tests. Compared with the wind tunnel tests, the computational fluid dynamics (CFD) approach was more convenient for the investigations of the local wind field. It was found that the influence of bridge tower on the wind flow can increase rapidly the wind speed on vehicles while bearing off a narrow zone near the tower. The dangerous situation can be effectively compromised by installing a proper local windshield barrier (WSB) with varying heights and porosity ratios along the bridge span. The length of the influence region of tower on the wind environment over the bridge deck was about 7 times of the tower width, implying a proper length of local windshield barriers on each side of the tower. Parametric studies demonstrated that the length of local WSB with different porosity ratios could affect the slope of equivalent wind speeds, indicating that the shorter the length of local WSB was, the rapider the wind speed of the tower influence region varied.

1. Introduction

Under the strong incident crosswind, vehicle handling becomes difficult affecting the safety statue of transportation vehicles significantly (Baker and Reynolds, 1992). Due to the aerodynamic forces in extreme wind conditions, high-sided vehicle can be blown off from its intended course and even overturned; smaller vehicles can suffer severe handling problems and may be pushed sideways by gust wind (Baker, 1987, 1998; Gawthrope, 1994). Both cases can result in multiple vehicle accidents which will cause traffic sudden stoppage, economic losses, injuries and even loss of lives.

Some statistical data of accidents show that vehicles on bridges under crosswind are more vulnerable to accidents than those on ground roads. There may be three major reasons as reported by some researchers (Charuvisita et al., 2004a, 2004b; Chen and Cai, 2004). Firstly, vehicles will suffer suddenly strengthened crosswind when passing through bridges over open terrains, compared with the case of vehicles on ground roads, especially for the case with trees, bushes or other barriers on both roadsides. Secondly, strong dynamic response of long-span bridge deck under crosswind and its coupling effect with vehicle vibration will amplify the vibration and reduce the stability of the vehicles moving on the bridges. Thirdly, for long-span cable-supported bridges, the shelter and interference effects of bridge tower on the incident crosswind will make the wind environment over the bridge deck within the region around the tower very severe, and the longitudinal variation gradients of both the wind speed and direction are often very significant. Therefore, while passing the tower region, vehicles will undergo a sudden drop of crosswind when entering the tower shading region and a sudden raise of crosswind when bearing off the tower region. This may cause miss-steering and severe driving accidents, and actually, many of this kind of accidents have been reported.

Computational Fluid Dynamics (CFD) has played an important role in wind environment and bridge engineering researches (Huang et al., 2009; Schmita et al., 2004; Shirai and Ueda, 2003). Large Eddy Simulation (LES) model is an important turbulent model of CFD which can calculate wind field around bluff bodies and complicated buildings with rather high precision. Simulation of the wind environment of tall buildings and the air flow around a long-span bridge deck have been carried out successfully by using LES turbulent models (Selvam et al., 1998; Watanabea and Fumotob, 2008).

In this work, LES turbulent model is employed to simulate the wind environment over bridge deck around the bridge tower by using FLUENT,

* Corresponding author.
E-mail address: zhouqi@stu.edu.cn (Q. Zhou).

https://doi.org/10.1016/j.heliyon.2020.e03902
Received 18 February 2019; Received in revised form 16 March 2020; Accepted 29 April 2020

a famous CFD software, and the simulated results are compared with those obtained via wind tunnel tests. Moreover, some factors such as width and shape of the bridge tower, speed and yaw angle of crosswind, and the length of local wind shield barriers, are also investigated using CFD approach.

2. Experiment setup

2.1. Engineering background and test models

The Xiangshan Harbor Bridge, a typical long-span highway bridge in China, was taken as an engineering background to investigate wind environment around bridge deck near tower. The structure is a cable-stayed bridge with a main span of 688 m and two side spans of 344 m, respectively. The bridge girder is classic streamed line single box, 34.0 m wide and 3.5 m high, having four lanes upon the bridge deck formed a dual two-lane highway. Four lanes are identified as lane1-4 in a sequence from windward to leeward in this present work. Each tower is a 234.3 m high concrete structure with a shape like a diamond. Figure 1 shows the cross section of main span in the bridge operation stage. There were some elements around the bridge deck, such as two central and two side guardrails, two maintenance tracks and the windshield barriers (WSB). The WSBs were consist of the normal WSB used in most of the bridge span and the local WSB used only in the region near the tower, both of which were employed to improve the wind environment over the bridge deck.

Figure 2 shows the layout of wind shield barriers near the tower. It is seen the WSB applied in Xiangshan Harbor Bridge consists of curved posts and horizontal rectangular wind-shelter laths. According to the porosity ratio (*Pr*) ranged from 10–60%, the WSB is divided into six types (interval of *Pr* is 10%). The WSB with *Pr* of 10–50% named local WSB and arranged in a sequence with *Pr* decreasing gradually. Each type of WSB is of 12 m long that means the total length of local WSB equals 120m. The length of local WSB on each side of tower was 60 m and was of a zigzag shape with two heights of 4.2 m and 3.6 m. The WSB with *Pr* of 60% was normal WSB in the height of 3.0 m and arranged in the rest mid-span of the bridge. Here it is noted that the normal WSB was upgraded form the handrail, thus the bottom part was still a handrail and the upper part was produced by several horizontal rectangular wind-shelter laths.

To simulate the dynamic behavior of bridge deck exactly, a large-scale bridge model has been designed for wind tunnel tests. The bridge model, composed of tower model segment and girder model segment, is made in ABS engineering plastic and adopted a geometric scaling factor of 1:25 after a careful consideration of many factors. The segmented tower model is 1.85 m high which is about 0.85 m upon the deck upper surface and 1.0 m below the deck upper surface. The segmented girder model, with a total length of 6.14m, is composed of a stationary part and a removable part which are 4.64 m and 1.5m, respectively. Taking the width of tower model as a representative length, 0.46 m, the dimensionless distance (Y/B, where Y is the distance away from the tower axis in the longitude direction and B is the width of tower model) is used in the following description. The maximum Y/B in the wind tunnel tests reached 11, while that in the CFD simulation was more than 13, which was in consideration of reducing 3D flow effect.

2.2. TJ-3 and measurement system

Wind tunnel tests were conducted in the TJ-3 wind tunnel of State Key Laboratory for Disaster Reduction in Civil Engineering at Tongji University in China. The TJ-3 wind tunnel is a closed type boundary layer wind tunnel with a working section of 15m wide, 2m high and 14m long. The achievable mean wind speed ranges from 1.0 to 17.6 m/s. The girder model was supported by several steel tubes and with a height of 1.0 above the tunnel floor. The tower model stands at the center of the turntable in TJ-3 (see Figure 3). To ensure the stability, tower model was pasted on a plastic plate at the bottom of tower legs and held against the tunnel by two small jacks on the top of tower legs. Indeed, the horizontal stiffness of the whole model was provided by the steel tubes and the tower model to ensure that the model is motionless in the entire test process.

As mentioned above, the girder model is composed of a stationary part and a removable part. While measuring the cross section with a dimensionless distance less than 4.5 (that is $Y/B < 4.5$), the removable and stationary parts were installed separately at different sides of the tower model (see Figure 3a) to reduce the end-effect of 3D flow. While measuring the cross section with Y/B larger than 4.5 ($4.5 \leq Y/B \leq 12$), the removable and stationary part were installed at the same side of the tower model (see Figure 3b).

Wind speed of the wind tunnel test was set as 10 m/s with a smooth wind field. In nominally smooth flow conditions, there is a residual along wind turbulence intensity 1 %, and a 1 % of mean velocity variation in the measurement section. Generally, the turbulence intensity at the site of sea-crossing or coastal bridge is about 6 %, which is a little higher than the turbulence intensity in the wind tunnel test. However, considering that the characteristics of the wind profile studied in this paper are the

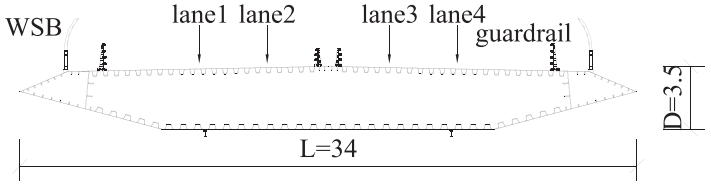

Figure 1. Cross section of main span of Xiangshan Harbor Bridge.

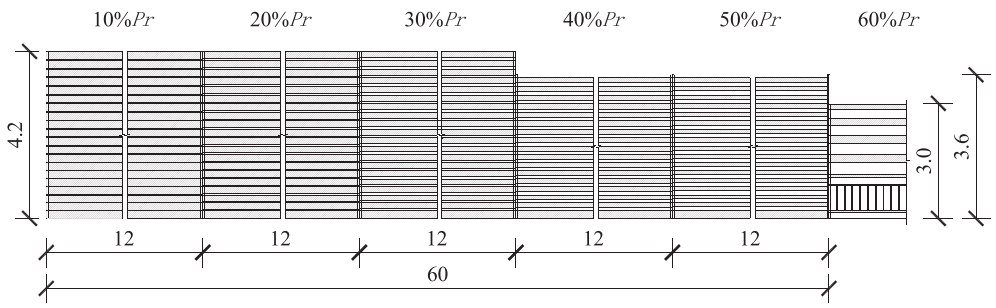

Figure 2. Layout of wind shield barriers near the tower.

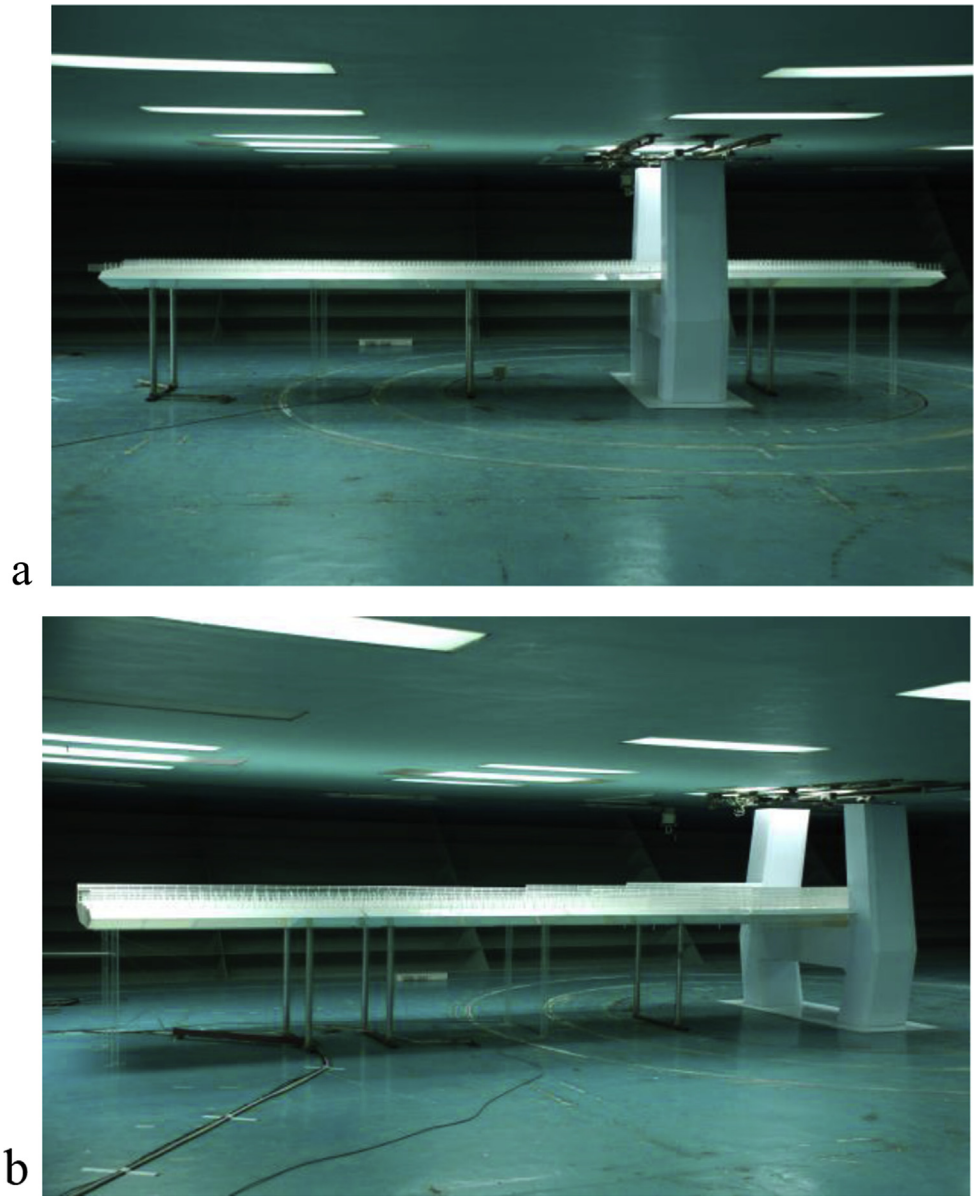

Figure 3. Test model in the wind tunnel TJ-3: (a) removable and stationary part on both sides; (b) removable and stationary part at the same side.

ratios of wind speed at different heights, the slightly larger turbulence intensity should have little impact on the wind speed ratios. Wind speed measurement system, consisted of an electronic pressure scanning valve system, a special wind speed probe and an automatic lifting system, was used in the wind tunnel tests. The special wind speed probe, combined with five Pito-static tubes (see Figure 4), is a customized product for the test. The distance between the tap centers of two adjacent Pito-static tubes was 5 cm. The wind speed probe was mounted at the front of a mechanical arm, which is driven by the lifting system and can move 2 mm per step accurately. Due to the special wind speed probe and the automatic lifting system, five points at different heights upon bridge deck can be measured synchronously and conveniently at each step of the mechanical arm movement. In order to ensure quality of test data, the wind speed probe was calibrated by a standard Pito-static tube in advance and all test data will be modified on the basis of calibration results.

3. Numerical simulations

3.1. LES governing equations

In LES method, eddies in the fluid are divided into larger-scale eddies and small-scale eddies by an implicit spatial filter. Large-scale eddies are solved directly and influences of small-scale eddies on large-scale eddies are modeled. Thus, filtered incompressible Navier-Stokes equations and filtered continuity equation are given as:

$$\frac{\partial \overline{u_i}}{\partial t}+\frac{\partial \overline{u_i u_j}}{\partial x_j}=-\frac{1}{\rho}\frac{\partial \overline{p}}{\partial x_i}+\frac{\partial}{\partial x_j}\left(\nu\frac{\partial \overline{u_i}}{\partial x_j}\right)-\frac{\partial \tau_{ij}}{\partial x_j} \tag{1}$$

and

$$\frac{\partial \overline{u_i}}{\partial x_i}=0 \tag{2}$$

Figure 4. The special wind speed probe.

where $\overline{u_i}$ and $\overline{p}$ are resolved filtered velocity and pressure, respectively. As described in Eq. (1), velocity can be divided into resolved part ($\overline{u}(x,t)$) and ($u'(x,t)$), and the unknown part ($\tau_{ij} = \overline{u_i u_j} - \overline{u_i}\,\overline{u_j}$), namely sub-gird-scale stresses (SGS). The unknown SGS represent the contribution of small-scale eddies to large-scale eddies, both of which are required to be modeled. Standard Smagorinsky Model, Dynamic Smagorinsky Model and WALE Model are three common SGS turbulence models and the first model is used in present study due to simplicity and cost effective of computational resources. In the Standard Smagorinsky Model, SGS is modeled as

$$\tau_{ij} - \frac{1}{3}\tau_{kk}\delta_{ij} = -2\mu_t \overline{S}_{ij} \tag{3}$$

where δ_{ij} is Kroneker symbol, and $\overline{S}_{ij}$, denotes the rate-of-strain tensor for the resolved scale, which is defined as

$$\overline{S}_{ij} = \frac{1}{2}\left(\frac{\partial \overline{u_i}}{\partial x_j} + \frac{\partial \overline{u_j}}{\partial x_j}\right) \tag{4}$$

According to the Smagorinsky-Lilly Model proposed by Smagorinsky (1963), the turbulent viscosity, μ_t, is defined as follows:

$$\mu_t = l^2|\overline{S}| \tag{5}$$

where$|\overline{S}| = \sqrt{2\overline{S}_{ij}\overline{S}_{ij}}$, and $l$is normal damping length scale by which the wall effects near the walls are partially taken into account. Based on Van Direst damping function l is defined as the follows

$$l = C_s\overline{\Delta}\left[1 - \exp\left(-\frac{y^+}{25}\right)\right] \tag{6}$$

where C_s is Smagorinsky model coefficient and considered to be 0.13 in present work. On structured grid, filter width $\overline{\Delta}$, can be calculated by $\overline{\Delta} = (\Delta x \Delta y \Delta z)^{1/3}$ and for unstructured grid, it is taken as cubic root of the volume of a finite volume cell.

3.2. Geometry description and calculation setup

Geometric scaling factor of the model in numerical simulation is still 1:25, which is the same as the wind tunnel test mentioned above. To reduce computation cost, only a segment of the bridge tower near the deck is taken into account in numerical analysis. Besides, in the consideration of structure symmetry, only a half structure of tower is modeled in this work. In the following description, breadth B of bridge tower and height D between upper and lower surface at deck center are regarded as two representative dimensions. Figure 5a depicts the segment of tower model which are both 7D high above and below the deck upper surface.

Indeed, the WSB model in CFD still adopted the same geometric scaling factor as the tower and bridge model. However, gap between original vents of some cases is too small to be simulated after scaling, thus some WSB model is simplified to reduce computation cost. Such as the WSB with porosity ratios of 10–30%, the number of wind-shelter laths in numerical model is reduced but general porosity ratio of WSB is kept unchanged by the method of enlarging the width of vent gaps. As is shown in Figure 5b, 9 rectangular laths are substituted for the original 18 laths of curved wind shield barriers with a porosity ratio 10%. In fact, this kind of aggregating method of porosity ratio similarity is also frequently adopted in scaled models of various ventilated parapets or windshield barriers for wind tunnel test. Moreover, the wind shield posts are not molded in CFD analysis for simplification because most parts of posts are sheltered by horizontal laths and sheltering areas of the rest parts of the posts are relatively small.

Besides the bridge without WSB, three kinds of local WSB near tower, including 40 m (=5 × 8 m)、60 m (=5 × 12 m), and 80 m (=5 × 16 m) are considered for CFD simulation. Wind yaw angles and wind attack angle considered are set as 0°. More details of the case studies and computational conditions are listed in Table 1:

It should be indicated here that in the present work, the Reynolds numbers of both the CFD simulations and the wind tunnel tests are a little smaller than 1×10^5(actually 93,800), which are suitable in the region of subcritical zone, whereas the Reynolds number of the prototype of WSB should be about2×10^6based on the same wind speed, which is suitable in the region of pre-critical zone. This is reasonable because both the bridge deck and the WSB is of the blunt bodies, implying that effects of the Reynolds number can hardly be serious and can be ignored. Furthermore, the present work focused on the possibility of the CFD simulations on the wind speeds behind the WSB and the interference of the bridge tower on wind speeds. In addition, previous studies have shown that the Reynolds effect was not very significant for the blunt body structure of the bridge section. Therefore, such an effect of the Reynolds number has not been considered in our simulations. In addition, the porosity ratios of the WSBs was kept the same as that in the prototype. It

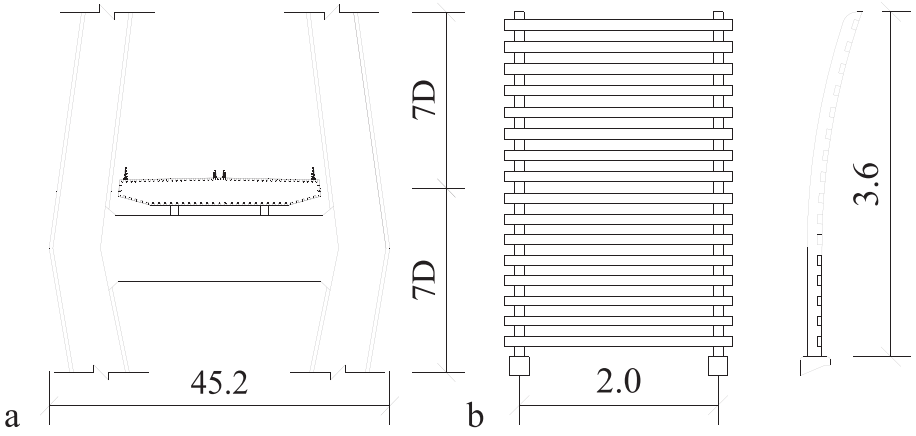

Figure 5. Elevation of tower segment and WSB with *Pr* of 10%: (a) tower segment; (b) WSB substitute treatment (Unit: mm).

Table 1. Computational parameters and conditions.

Calculated model cases		Computational conditions	
Tower shape	diamond	Number of elements per case	$6\times10^6$1.4$\times10^7$
Tower breadth	11.5 m	Reynolds number, *Re*	about 100,000
Wind speed	25 m/s	Time increment	0.005*D*/*U*
Wind Yaw/attack angle	0°	Smagorinsky constant C_s	0.13
Length of WSB	40m, 60m and 80m	Blockage ratio	0.04
Height and porosity ratio of WSB	4.2m (Pr = 10–30%), 3.6m (Pr = 40–50%) and 3.0m (Pr = 60%)	CPU	X5570 2.93GHz
		Number of nodes	8
		Memory	DDR3-1333 12GB

should also be noted that due to the gap between the adjacent laths of the WSB (Pr = 10%) was too small to obtain precisely, the numbers of the laths have been decreased and the widths of laths have been increased, but the porosity ratio was still 10%.

3.3. Boundary conditions

X and *Y* axes in the numerical model are along lateral and longitudinal directions of the bridge span, respectively. Indeed, axis *X* also indicates the streamwise direction, and *Z* axis represents the vertical direction. Figure 6a shows computational cubical domain which is 75D (height of girder) in length, 14D in height, and 12B (breadth of tower) in width. Besides, the bridge girder model is 25D and 50D away from the left and the right surface of the computational domain, respectively. There are four types of boundary conditions applied at six surfaces of computational domain. As can be seen in Figure 6b, the flow enters the cuboid domain with a uniform velocity profile constant in time, which means the velocity inlet of 10 m/s is set as the boundary condition of windward surface. For the leeward surface where the flow leaves domain, pressure outlet condition with the normal gradients of the velocities selected to be zero is employed. The symmetric boundary condition is used for top and bottom, left and right surfaces of the domain. In addition, the no-slip wall condition is applied on the surfaces of bridge girder and tower. Implementation details of the wall functions can be found in Krajnovic and Davidson (2003).

3.4. Mesh

The models were meshed by the tool of ANSYS and ICEM, and two different kind of meshes were generated: a coarse mesh containing 6.0×106 cells and a fine mesh containing 1.4×107 cells. The meshes were generated primarily with structured hexahedral cells, however, there also was a number of unstructured prisms and polyhedral cells in the complicated geometry zone, especially around the bridge tower. Figure 7a and Figure 7b show the mesh slices at the center of bridge tower with a fine mesh and a coarse mesh. Figure 7c and Figure 7d show the mesh slices of bridge girder with a fine mesh and a coarse mesh.

The auto adaption function was activated to re-mesh the cells to ensure the size of the smallest turbulent scales that can be solved. Thus, it is necessary to ensure that the cell size is sufficiently small to capture the smallest energy containing eddies. The normalized wall distance, defined by y+, was employed to ensure the smallest eddies can be solved. 75% of the cells showed a y + value less than 3. However, there were a few cells at the gap between bridge tower and bridge girder that showed a higher y + value, and their maximum was 15.2. The mean values are shown in Table 2.

Finally, it is noted here that we also tried other turbulence models with fine and coarse mesh schemes, such as k-ε model. Furthermore, we compared the results from LES model with those from the k-ε model and found that based on the results from the k-ε model, there was a great deviation with the wind tunnel tests.

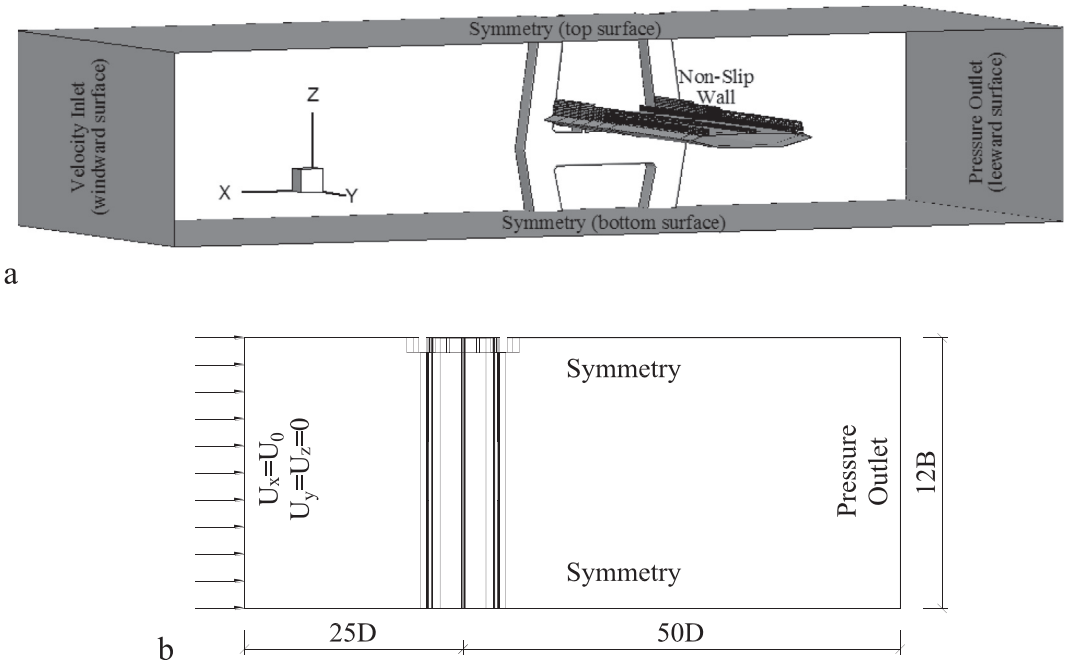

Figure 6. Solution domain and boundary conditions: (a) Three-dimension outline; and (b) a XZ slice.

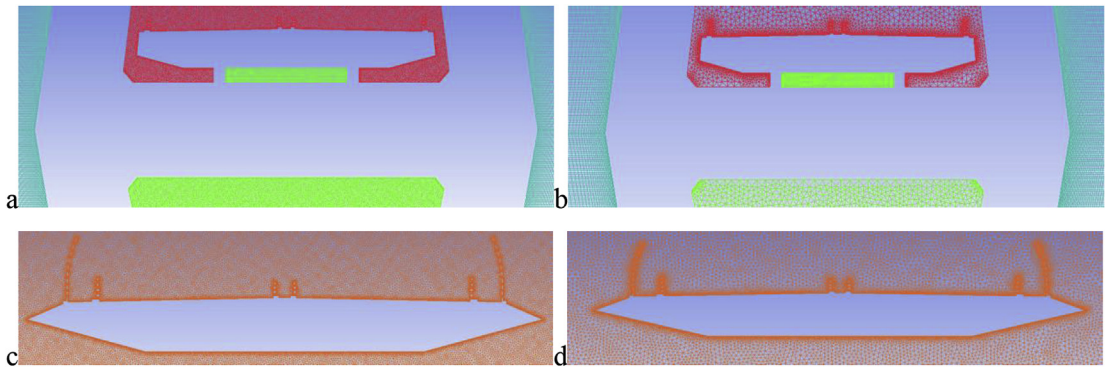

Figure 7. Meshing details: (a) slice at the center of tower with the fine mesh; (b) slice at the center of tower with the coarse mesh; (c) slice of bridge girder with the fine mesh; and (d) slice of bridge girder with the coarse mesh.

Table 2. Average value for the normalized wall distance.

	LES Fine	LES Coarse	k-εFine	k-εCoarse
y+	10.23	11.45	6.67	7.42

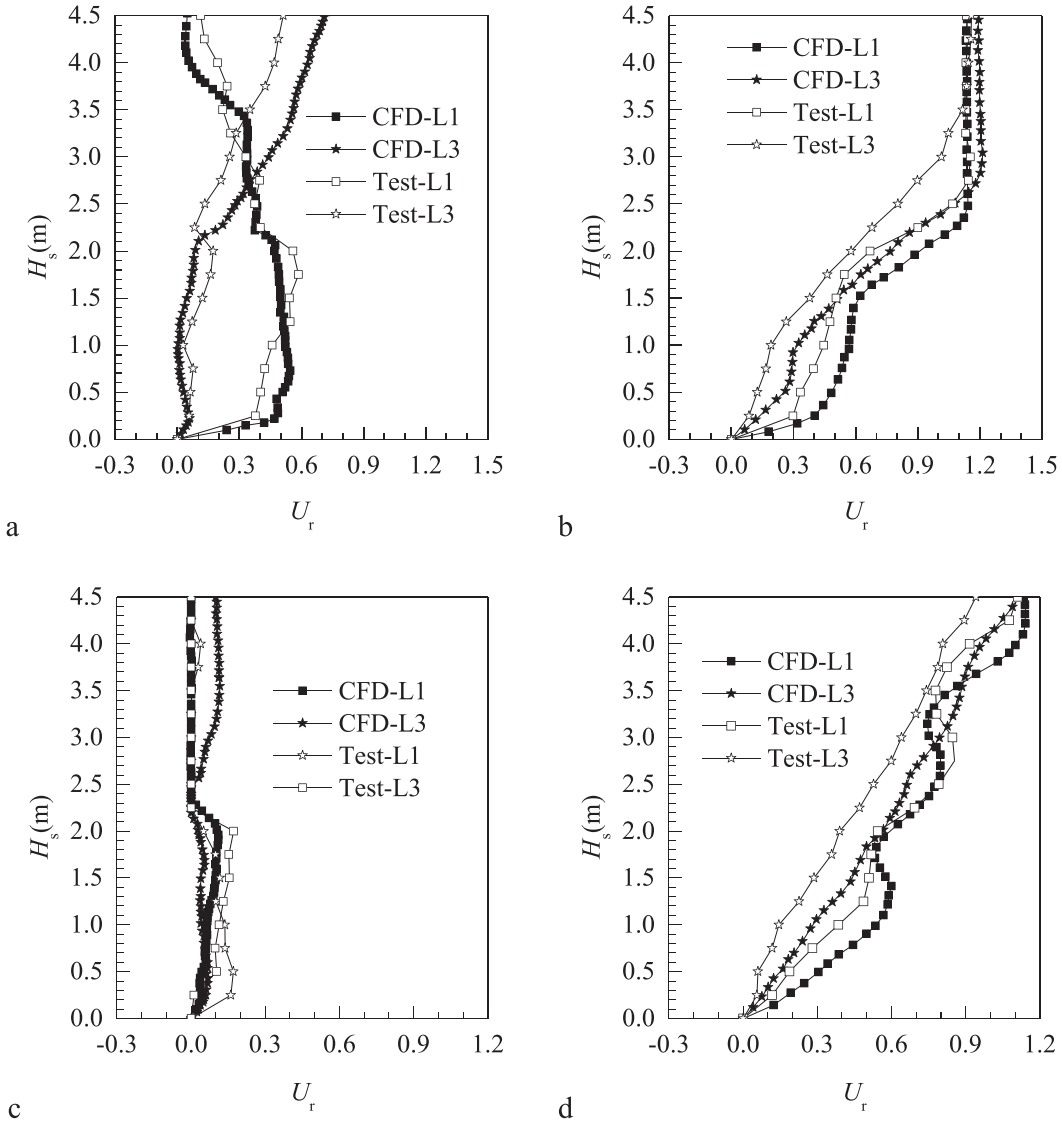

Figure 8. Wind profile comparison form wind tests and CFD results: (a) Dr = 0.5, no WSB; (b) Dr = 8; no WSB; (c) Dr = 0.5; local WSB; (d) Dr = 8; local WSB.

4. Results and discussions

4.1. Wind profile of vehicle lanes

Figure 8 shows wind profiles over the bridge deck at the center of 1st and 3rd vehicle lanes (see Figure 1) obtained by wind tunnel test and CFD computation. Figure 8a and Figure 8b are the results without local WSB and Figure 8c and Figure 8d are the results with local WSB. In this figure, H_s refers to the height above the deck surface; $U_r = U_s/U_0$ is dimensionless relative wind speed; U_s denotes the horizontal mean wind speed along normal direction of bridge span; U_0 is the mean speed of incident wind; D_r is the distance between concerned girder section and tower central plane.

It can be seen from Figure 8 that wind profiles obtained by CFD has similar variation tendency along height to those obtained via wind tunnel test and calculated relative wind speed (U_r) was generally slightly larger than the tested ones. It can be also found that in Figure 8a, for wind profiles at the section of $D_r/B = 0.5$ (at the edge of tower) and without local WSB, variation pattern of U_r along height was rather complex and exhibits a nonlinear manner. As for the windward lane 1, although the variation of U_r was remarkable, the values of CFD results and wind tunnel tests matched well with each other. While the height was less than 2.0 m which was a little higher than the heights of guardrails and handrails, the U_r mainly keeped close to 0.5, and while the height was larger than 2.0 m, the U_r decreased with the increasing of height. As for the leeward lane 3, the values of CFD results and wind tunnel tests also matched well under the height of 2.0 m, but the CFD results were much larger than those of wind tunnel tests over the height of 2.0 m. This may be because the direction of wind in this region deviates severely from the normal of bridge span, leading to significant measurement error of wind speed using Pito-static tube.

As shown in Figure 8b, for the case of $D_r/B = 8$ (relatively far away from the tower) and without local WSB, each wind profile approximately consists of three segments. Within the first segment whose height was lower than 1.5 m, wind speed was relatively low due to the shelter of guardrails and handrails, but generally increased as height exceeded 1.5 m. With the second segment whose height was between 1.5 m and 2.8 m, the wind speed increased rapidly because of the vanishing of the shelter effect of guardrails and handrails. As for the third segment whose height was larger than 2.8 m the wind speed was almost constant against the height and the influence of girder on wind speed can be ignored.

Figures 8c and 8d show the wind profiles at sections of Dr/B = 0.5 and Dr/B = 8 with local WSB. As can be seen from Figure 8c, the wind speeds of CFD results were close to those of wind tunnel tests although the variation of wind speeds were still dramatically. Compared with Figure 8a, the local WSB significantly decreased the value of U_r over the section $D_r/B = 0.5$ with the maximal value being about 0.2. This indicates that the crosswind on vehicles can be significantly weakened by installing local WSB, especially for the vehicles on windward lanes. It is worth mentioning that due to the wind direction may be not along the installed direction of Pito-tube, the results of 0 in the wind tunnel test didn't mean the real wind speed was zero. In addition, it is also found that the second segment of wind profiles occurring in Figure 6b disappeared in Figure 8b due to the local WSB, which generated the relatively smooth wind profiles, especially for that over the leeward lane (lane 3).

As shown in Figure 8b, the wind speeds simulated by CFD were obvious larger than those obtained by the wind tunnel tests, especially for the results of windward lane (lane 1). As for lane 1, the wind speed increased gradually with the increment of height, and almost showed with a linear characteristic. As for lane 3, the wind speeds were remarkable fluctuant but mainly increased with the increasing of height However, it can be concluded that with the height continuously increased, the wind speed would keep constantly.

In conclusion, due to the shelter effect of the local WSB, the wind profiles over bridge deck become gently and smooth. This also indicates crosswind on vehicles can be significantly weakened by installing local WSB and the wind environment over bridge deck can be improved, especially for the vehicles on windward lanes.

4.2. Equivalent wind speed

It can be seen from the above results that the wind speed over vehicle lanes varies with height due to the influence of bridge girder, tower, guardrails and handrails. Therefore, it is necessary to introduce an equivalent wind speed to evaluate the effectiveness of windshield barriers on the safety of vehicles moving on various deck lanes. An equivalent wind speed (U_{equ}) used in this study is based on the approximate equivalency of lateral aerodynamic force on vehicles and is defined as follows:

$$U_{equ} = \sqrt{(1/H_{max}) \int_0^{z_r} U^2(z)dz} \tag{7}$$

where $U(z)$ is wind pressure at the height of z; H_{max} is maximal height of vehicles. Usually, the height of heavy vehicles is less than 4.5 m, so that H_{max} is assumed to be 4.5 m in this study. Dimensionless coefficient of equivalent wind speed, which is often employed to evaluate wind environment over bridge deck for vehicle driving and the effectiveness of windshield barriers, can be determined as follows:

$$\lambda = U_{equ}/U_0 \tag{8}$$

Figure 9 shows the calculated and tested curves of λ vs. D_r for the cases without local WSB and under normal wind, where D_r is dimensionless distance of the concern section from tower center, and is equal to D_r/B. It is seen that the curves of λ vs. D_r obtained by CFD had a similar variation pattern with those of wind tunnel tests and were also somewhat higher than the tested values. The major reason of this occurred phenomenon may be that, the actual direction of wind over bridge deck deviated from both the horizontal plane and normal direction of the bridge span, which were inconsistent with the axis of the Pito-static tubes. This will lead to a tested wind speed underrated to some extent. Moreover, the ignorance of windshield barriers, guardrails and handrails in the CFD analysis slightly overestimate the calculated wind speed.

As shown in Figure 9, equivalent wind speed at tower center section was very small and less than 30% of incident wind speed due to the shelter effect of tower. However, the equivalent wind speed increased rapidly as vehicle moved out of the tower, and reached the maximum value, which was about 100%–120% of incident wind speed for different lanes within a narrow zone just out of the tower edge (while D_r is between 1.0 and 1.5). The equivalent wind speed values dropped at an almost consistent decreasing rate as the distance increased from the tower center, approaching a stable level (about 90%–100%) when vehicles drove far away from the tower. Based on, the influence region of bridge tower can be roughly divided into two zones based on the variation trends of λ curves shown in Figure 9: namely the shadow zone (D_r<1–1.5 in normal wind case) with a rapid increase of λ; and bypass flow zone (neighbor to the shadow zone) with a gradual decrease ofλ.

It can be also found in Figure 9 that wind speed equivalent coefficients of 1st lane were close to that of 4th lane and wind speed equivalent coefficients of 2nd lane were close to that of 3rd lane, indicating that the wind environment at the center of bridge deck varies slightly with stable wind environment. Moreover, wind speed at the border of bridge deck was larger than that at the center of bridge deck and wind environment at the border of bridge deck was relatively dangerous.

4.3. Shielding effects of WSB near tower

4.3.1. The case installed with local WSB

Figure 10 presents the calculated and tested curves of λ vs. D_r for the cases without local WSB under normal wind. Compared with

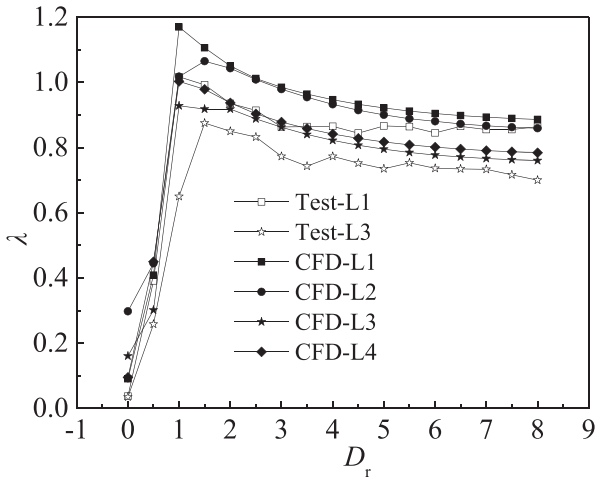

Figure 9. Wind speed equivalent coefficient results for the case without WSB. 1.0.

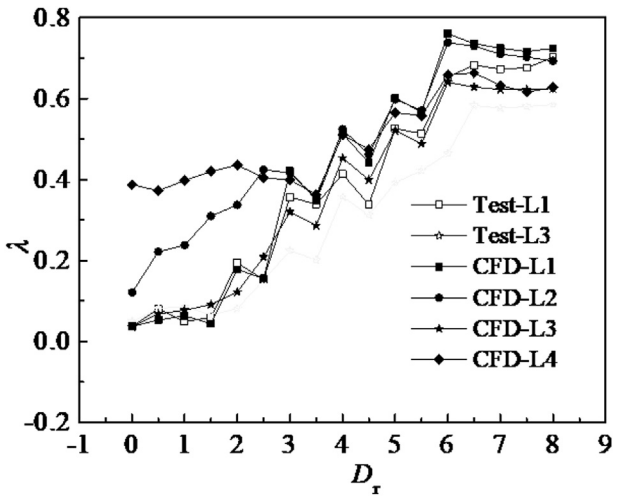

Figure 10. Wind speed equivalent coefficient results for the case with WSB.

Figure 9Figure 9 and Figure 10Figure 10, it can be seen that installation of a proper local WSB can effectively eliminate the above phenomena of rapid rise of equivalent wind speed near bridge tower, so that vehicles at the tower region may bear less external force induced by increased wind speed. Interference of the bridge tower on the wind flow limited the gradient of wind speed within a narrow zone near the bridge tower, resulting in a very dangerous wind environment region to driving vehicles. This dangerous wind environment can be effectively improved by installing proper local WSB.

It can also be seen in Figure 10 the curves of λ vs. Dr become serrate after installing the local WSB. This phenomenon may be attributed to two reasons, the change of height and porosity ratio of the local WSB along the bridge span was not continuous and the presence of vortex shedding in horizontal plane. It is also worth to note that, after the installation of local WSB, equivalent wind speed over the 2nd lane and the 4th lane were much higher than those over the other two lanes, especially for the sections with lower values of D_r, where, the WSB was high and had low porosity ratio. This is because the 1st and 3rd lanes are relatively closer to the local WSB or the central guardrail than the other two lanes, leading to shelter effect of the laths of WSB or guardrail is more significant on the wind over the 1st and 3rd lanes than on that on the wind over the other two lanes.

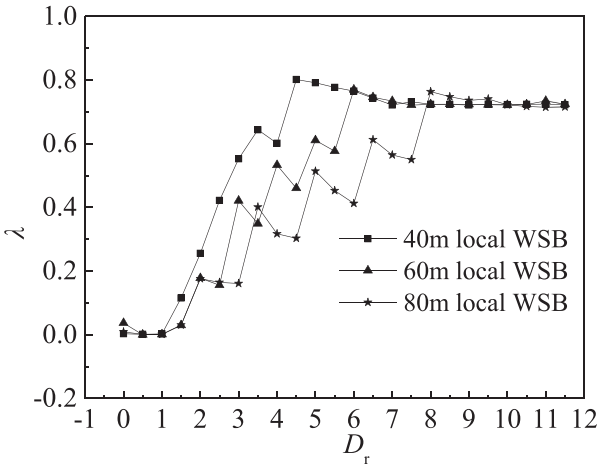

Figure 11. Wind speed equivalent coefficients of local WSB with different lengths.

In the region near the bridge tower (while Dr < 3.5), wind speed equivalent coefficients of 1st lane were close to that of 3rd lane, while wind speed equivalent coefficients of lane1 became close to that of 2nd lane and wind speed equivalent coefficients of 3rd lane also got close to that of lane 4 when Dr is larger than 3.5. This was quite different from the results of the case without WSB. In terms of the WSB shielding effect, the wind environment of windward half bridge was better than that of leeward half bridge especially in the region near the bridge tower. In general, wind environment of leeward half bridge was worse than that of windward half bridge after installing WSB.

4.3.2. Comparison between different length local WSB

To investigate the influence of local WSB length on the improvement efficiency of the wind environment near bridge tower, three local WSB lengths, including 40 m (3.5 times of the tower width), 60 m (5 times of the tower width) and 80 m (7 times of the tower width) in one side of bridge tower, are taken into consideration by CFD method in this study. Figure 11 shows wind speed equivalent coefficient curves with respect to D_r of the 1st lane for the three kinds of local WSB. It is seen that the installation of local WSB enlarged the shadow zone of tower as the length of WSB increased. Increasing rate of λ with respect to D_r dropped in the shadow zone. Furthermore, as the increase of the local WSB length, both the maximum value and the increasing rate of λ descended whilst the length of local WSB just rose a bit. These results verified that the longer the local WSB, the smaller the general gradient of equivalent wind speed, and also the better the local wind environment. Therefore, in the consideration of both economy and safety of vehicle driving, the influence region length of tower (about 7B) is suggested as a proper length for the local WSB.

5. Conclusions

The local wind environment over the deck near bridge tower is investigated using the Numerical analysis and the wind tunnel test taking into account the effect of local windshield barriers on the wind environment improvement. Major concluding remarks are drawn as follows:

(1) Existence of bridge tower has significant influence on the wind flow field. Wind seed near the bridge tower presents a significant rise within a distance 12 times longer of tower width, posing a dangerous wind environment to vehicles. In this region, wind speed rises rapid and suddenly, Wind speed gradually decreases until the influence of bridge disappears.
(2) Influence of bridge tower on wind speed can be effectively weakened by installing proper local WSB with varying height and

porosity ratio along bridge span. Length of the influencing region of tower on the wind speed over bridge deck is about 7 times of the tower width, which is also the suggested proper length of local windshield barriers on one side of the tower.

(3) For the bridge without WSB, wind environment at the border of bridge deck is more dangerous than that at the center of bridge deck. After installing WSB, wind environment of windward half bridge is better than that of leeward half bridge.

Declarations

Author contribution statement

Q. Zhou: Conceived and designed the experiments; Analyzed and interpreted the data; Contributed reagents, materials, analysis tools or data; Wrote the paper.

L. D. Zhu: Performed the experiments.

Funding statement

This work is partially supported by China National Science Foundation (Grant No. 51308330), National Science Foundation of Guangdong province (Grant No. 2018A030307008), State Key Laboratory of Disaster Reduction in Civil Engineering, Tongji University (Grant No. SLDRCE18-01), which are gratefully acknowledged. Any opinions or conclusions presented in this paper are entirely those of the authors.

Competing interest statement

The authors declare no conflict of interest.

Additional information

No additional information is available for this paper.

References

Baker, C.J., 1987. Measures to control vehicle movement at exposed sites during windy periods. J. Wind Eng. Ind. Aerod. 22, 151–161.

Baker, C.J., Reynolds, S., 1992. Wind-induced accidents of road vehicles. Accid. Anal. Prev. 24 (6), 559–575.

Baker, C.J., 1998. The effects of high winds on vehicle behavior. In: Proceedings of International Symposium on Advances in Bridge Aerodynamics, pp. 267–282. Copenhagen, Balkema.

Charuvisita, S., Kimurab, K., Fujinoc, Y., 2004a. Effects of wind barrier on a vehicle passing in the wake of a bridge tower in cross wind and its response. J. Wind Eng. Ind. Aerod. 92, 609–639.

Charuvisita, S., Kimurab, K., Fujinoc, Y., 2004b. Experimental and semi-analytical studies on the aerodynamic forces acting on a vehicle passing through the wake of a bridge tower in cross wind. J. Wind Eng. Ind. Aerod. 92, 749–780.

Chen, S.R., Cai, C.S., 2004. Accident assessment of vehicles on long-span bridges in windy environments. J. Wind Eng. Ind. Aerod. 92, 991–1024.

Gawthrope, R.G., 1994. Wind effects on ground transportation. J. Wind Eng. Ind. Aerod. 52, 73–92.

Huang, W.R., Yang, Q.P., Xiao, H., 2009. CFD modeling of scale effects on turbulence flow and scour around bridge piers. J. Comput. Fluids 38, 1050–1058.

Krajnovic, S., Davidson, L., 2003. Numerical study of the flow around the bus-shaped body. ASME J. Fluid. Eng. 125, 500–509.

Schmita, R.F., Glauserb, M.N., Ahmadia, G., 2004. Flow and turbulence conditions in the wake of a H-section in cross flow. J. Fluid Struct. 19, 193–207.

Selvam, R.P., Tarini, M.J., Larsen, A., 1998. Computer modeling of flow around bridges using LES and FEM. J. Wind Eng. Ind. Aerod. 77&78, 643–651.

Shirai, S., Ueda, T., 2003. Aerodynamic simulation by CFD on flat box girder of super-long-span suspension bridge. J. Wind Eng. Ind. Aerod. 91, 279–290.

Smagorinsky, J., 1963. General circulation experiments with the primitive equations. Mon. Weather Rev. 91, 99–165.

Watanabea, S., Fumotob, K., 2008. Aerodynamic study of slotted box girder using computational fluid dynamics. J. Wind Eng. Ind. Aerod. 96, 1885–1894.